ARTICLE   OPEN

Superconducting order from disorder in 2H-TaSe$_{2-x}$S$_x$

Lijun Li[1,2], Xiaoyu Deng[3], Zhen Wang[1], Yu Liu[1], Milinda Abeykoon[4], Eric Dooryhee[4], Aleksandra Tomic[5], Yanan Huang[1,8], John B. Warren[6], Emil S. Bozin[1], Simon J. L. Billinge[1,5], Yuping Sun[2,7], Yimei Zhu[1], Gabriel Kotliar[1,3] and Cedomir Petrovic[1]

We report on the emergence of robust superconducting order in single crystal alloys of TaSe$_{2-x}$S$_x$ ($0 \leq x \leq 2$). The critical temperature of the alloy is surprisingly higher than that of the two end compounds TaSe$_2$ and TaS$_2$. The evolution of superconducting critical temperature $T_c(x)$ correlates with the full width at half maximum of the Bragg peaks and with the linear term of the high-temperature resistivity. The conductivity of the crystals near the middle of the alloy series is higher or similar than that of either one of the end members 2H-TaSe$_2$ and/or 2H-TaS$_2$. It is known that in these materials superconductivity is in close competition with charge density wave order. We interpret our experimental findings in a picture where disorder tilts this balance in favor of superconductivity by destroying the charge density wave order.

INTRODUCTION

The interplay of disorder and interactions is a fruitful area of investigation. In the absence of electron–electron interactions, disorder can turn a metallic system into an Anderson insulator,[1] but can remain metallic when interactions are important. The additional complexity of competing orders such superconductivity with charge density wave (CDW) or magnetism makes this problem one of the most challenging frontiers in physics.[2–5] A large body of literature is devoted to this interplay in nearly magnetic materials.[6] The interplay of disorder and superconductivity in CDW materials have been less explored than its magnetic analog.

Superconductivity and CDW are traditionally viewed as weak-coupling Fermi surface instabilities due to electron–phonon coupling.[7] Arguments have been made both for their cooperation and competition.[8, 9] Hexagonal transition metal dichalcogenide 2H-TaSe$_2$ (*P63/mmc* space group) undergoes a second-order transition to an incommensurate CDW at 122 K followed by a first-order lock-in transition to a commensurate CDW (CCDW) phase at 90 K, eventually becoming superconducting below 0.14 K upon cooling.[10, 11] 2H-TaS$_2$ has $T_c = 0.8$ K below an in-plane CCDW at 78 K.[10, 12] The CDW mechanism in 2H-TaSe$_2$ involves an electron instability in the bands nested away from the Fermi surface, whereas 2H-TaS$_2$ features a polar charge and orbital order.[13, 14] CDW in 2H-TaSe$_2$ is dominated by hopping between next-nearest neighbors that creates three weakly coupled triangular sublattices.[15] It is of interest to note that the 2H-TaSe$_2$ is quasi-two-dimensional (2D) metal with pseudogap and with c-axis resistivity 25–50 times higher than the in-plane resistivity, i.e., $\rho_c(T) \gg \rho_{ab}(T)$.[10, 13, 16–18]

Here, we report that in the 2H-TaSe$_{2-x}$S$_x$ alloy series the CDW is suppressed and the superconductivity is maximized with crystallographic disorder. The $T_c(x)$ evolution is correlated with the high-temperature linear resistivity $\rho(T) = aT + b$. The constant term b can be attributed to impurity-like carrier scattering of the local CDW fluctuations, and it also appears in dynamical mean field theory (DMFT) of bad metals at high temperature.[19–22] On very general grounds (Anderson theorem) s-wave superconductivity is immune to weak disorder,[23] on the other hand disorder is detrimental to CDW. We argue that the increase in superconducting T_c in the alloy is a direct result of disorder-induced suppression of CDW order. In a weak coupling picture, CDW suppression results in an increase in number of carriers available for superconductivity pairing at Fermi surface, thus enhancing T_c. The physical scenario that in systems where CDW competes with superconductivity disorder promotes the latter is very general and extends to a strongly coupled situation as long as disorder remains weak (see Supplementary Information).

RESULTS

Powder patterns for all samples have been successfully indexed within the *P63/mmc* space group. Representative refinement is shown in Fig. 1a and the unit cell is shown in Fig. 1b. Single crystal X-ray diffraction (XRD) patterns for a subset of single crystals used in this study (Fig. 1c) show (00l) reflections. Reflections shift to higher scattering angles with increasing S, indicating decrease of the unit cell volume. Evolution of unit cell parameters with S, obtained from fits to the powder patterns (Fig. 1d, e), is consistent with the single crystal data.

The resistivity of all single crystals (Fig. 2a) is metallic. The curves for $0 \leq x \leq 0.25$ show a change of slope in $\rho(T)/\rho(200\,\mathrm{K})$ (Fig. 2b). As opposed to commonly observed increase in $\rho(T)$ at T_{CDW} the slope change is attributed to CDW transition that leaves the bands

[1]Condensed Matter Physics and Materials Science Department, Brookhaven National Laboratory, Upton, NY 11973, USA; [2]Key Laboratory of Materials Physics, Institute of Solid State Physics Chinese Academy of Sciences, Hefei 230031, China; [3]Department of Physics & Astronomy, Rutgers, The State University of New Jersey—Piscataway, Piscataway, NJ 08854, USA; [4]Photon Sciences Directorate, Brookhaven National Laboratory, Upton, NY 11973, USA; [5]Department of Applied Physics and Applied Mathematics, Columbia University, New York 10027, USA; [6]Instrumentation Division, Brookhaven National Laboratory, Upton, NY 11973, USA and [7]High Magnetic Field Laboratory, Chinese Academy of Sciences, Hefei 230031, China
Correspondence: Lijun Li (lilijun@issp.ac.cn) or Cedomir Petrovic (petrovic@bnl.gov)
[8]Present address: Key Laboratory of Materials Physics, Institute of Solid State Physics, Chinese Academy of Sciences, Hefei 230031, China

Received: 15 August 2016 Revised: 3 January 2017 Accepted: 24 January 2017
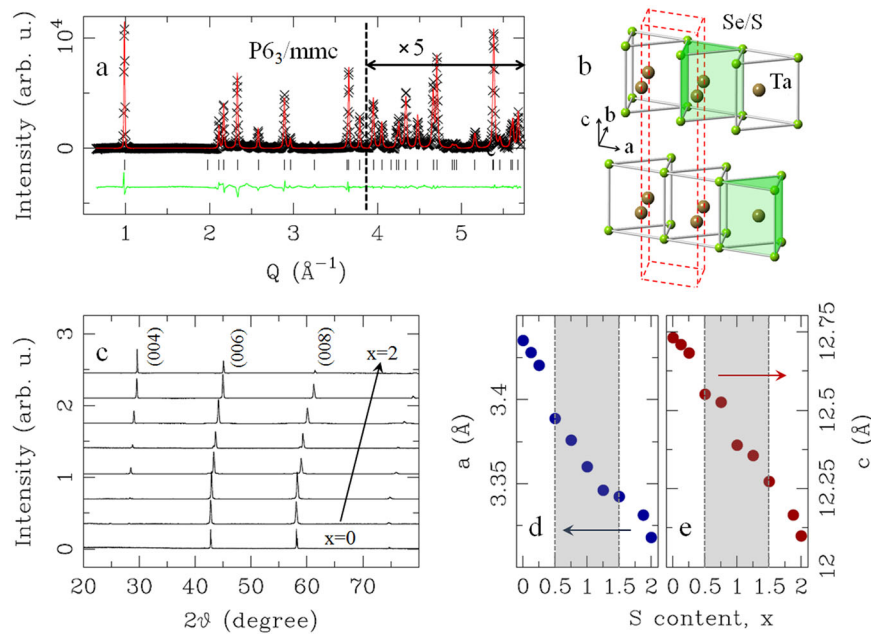Published online: 24 February 2017

Fig. 1 Crystal structure aspects of 2H-TaSe$_{2-x}$S$_x$ ($0 \leq x \leq 2$) **a** Powder XRD pattern for 2H-TaSe$_2$ at 300 K, shown as scattering intensity vs. momentum transfer Q, indexed within *P63/mmc* space group. *Crosses* are data, *solid red line* is the model, *green solid line* is the difference (offset for clarity), and *vertical ticks mark* are the reflections. **b** Structural motif of the *P63/mmc* model. *Red dashed box* depicts the unit cell. **c** Single crystal XRD patterns at the room temperature. Patterns are offset for clarity. **d**, **e** Room temperature evolution of *a* and *c* lattice parameters, respectively, as obtained from powder diffraction data. *Shaded* is the range where CDW cannot be detected in resistivity
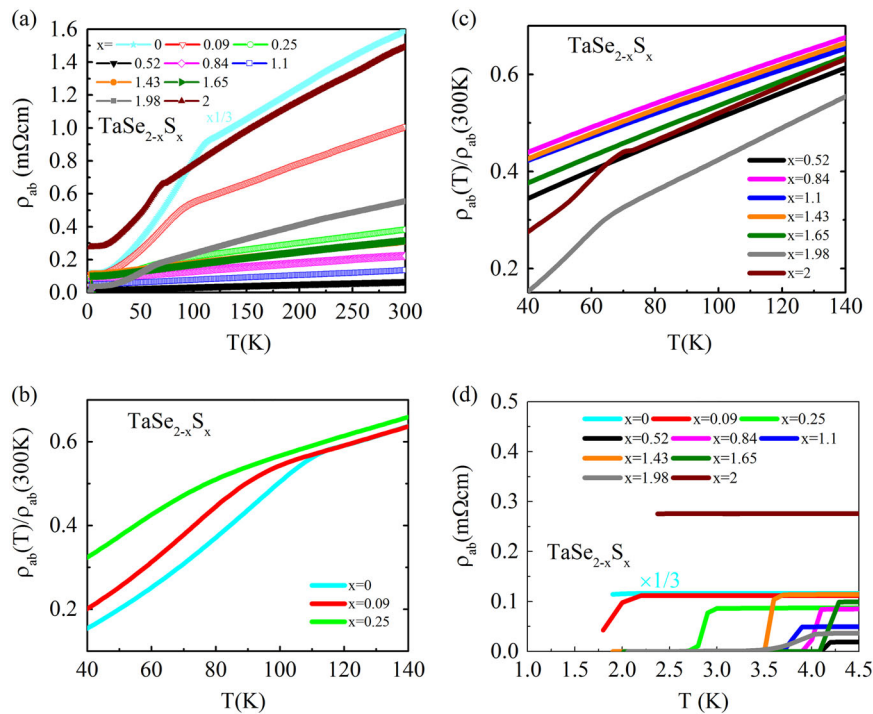

Fig. 2 Electrical resistivity of 2H-TaSe$_{2-x}$S$_x$ ($0 \leq x \leq 2$) **a** Temperature dependence of the resistivity for single crystals in the absence of magnetic field. **b**, **c** Temperature dependence of $\rho(T)/\rho$ (300 K) near CDW transitions. **d** $\rho(T)$ curves near superconducting transitions, indicating large enhancement of superconductivity

associated with the undistorted sublattice ungapped.[14–17] The hump shifts to lower temperature with S doping and vanishes for $x \geq 0.52$, but appears again for $x = 1.98$ at about 70 K, somewhat below the $T_{CDW} = 75$ K for pure 2H-TaS$_2$ (Fig. 2c). The

resistivity decreases to zero at lower temperatures, implying superconductivity (Fig. 2d). The magnetic susceptibility transitions and the large values of $-4\pi\chi$ at 1.9 K imply bulk superconductivity (Fig. 3a).
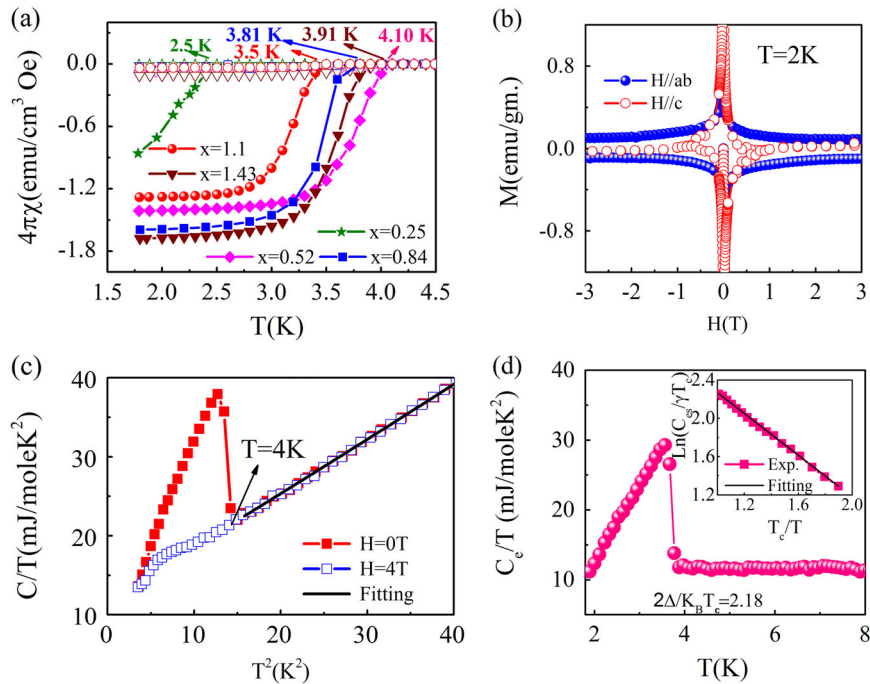
Fig. 3 Magnetic and thermodynamic properties of 2H-TaSe$_{2-x}$S$_x$ ($0 \leq x \leq 2$) **a** Magnetic susceptibility after zero-field-cooling (*filled*) and field-cooling (FC, *open symbols*). The smaller magnetization value for FC is likely due to the complex magnetic flux pinning effects. **b** Magnetization hysteresis loops M(H) of TaSe$_{1.48}$S$_{0.52}$ for H || ab (*solid*) and H || c (*open symbols*). **c** Low-temperature specific heat of TaSe$_{1.48}$S$_{0.52}$ measured at H = 0 (*solid*) and in 4 T (*open symbols*). **d** The electronic-specific heat in the superconducting state C_e for 2H-TaSe$_{1.48}$S$_{0.52}$ is obtained by subtracting the lattice contribution from the total specific heat: $C_e = C - C_{ph} = \gamma T$, where $C_{ph}(T) = \beta T^3 + \delta T^5$ and $\theta_D = [(n \cdot 1.944 \times 10^6)/\beta]^{1/3}$, where n is the number of elements per formula unit. *Inset*: below the superconducting transition temperature, electronic-specific heat temperature dependence follows an exponential decay, as $C_e \sim \exp[-\Delta(T)/k_B T]$. The *solid line* shows C_e/T calculated by assuming an isotropic s-wave BCS gap with $2\Delta = k_B T_c = 2.17$

Parameters	2H-TaSe$_2$	2H-TaSe$_{1.48}$S$_{0.52}$	2H-TaS$_2$
T_c(K)	0.14	4.20(1)	0.8
γ (mJ/mol K^2)	4.5	12.0(3)	7.5
β (mJ/mol K^4)	0.72	0.65(2)	0.44
δ (mJ/mol K^6)	–	6(1)·10^{-4}	–
λ_{e-ph}	0.397	0.73(1)	0.486
θ_D(K)	202	207(1)	236
$2\Delta/k_B T_c$	–	2.18(2)	–
Reported by	Ref 12	This work	Ref 12

Specifically, the anisotropic M(H) curves (Fig. 3b) confirm type-2 superconductivity for TaSe$_{1.48}$S$_{0.52}$ and imply anisotropic critical current density. The lambda anomaly in the specific heat jump around $T = 4$ K (Fig. 3c) is suppressed significantly in 4 T. A rough estimate of the average electron–phonon coupling $\lambda_{e-ph} \sim 0.73^1$ can be obtained from the McMillan equation, assuming the empirical value of the Coulomb pseudopotential $\mu^* = 0.15$ and taking the Debye frequency as the relevant phonon energy:[24]

$$\lambda = \frac{\mu^* \ln\left(\frac{1.45T_c}{\theta_D}\right) - 1.04}{1.04 + \ln\left(\frac{1.45T_c}{\theta_D}\right)(1 - 0.62\mu^*)}. \quad (1)$$

When compared with the parent 2H-TaSe$_2$ with electronic-specific heat coefficient $\gamma = 4.5$ mJ mol^{-1} K^{-2}, γ is larger for 50% S-doped sample (Fig. 3d, Table 1). The electron–phonon coupling $\lambda_{e-ph} = 0.73$ is somewhat larger than for 2H-TaSe$_2$ and 2H-TaS$_2$

(Table 1). The ratio of the gap at the critical temperature $2\Delta/k_B T_c = 2.17$ can be obtained by linear fitting $\ln(C_e/\gamma T_c) - T_c/T$ data (Fig. 3d inset).

In a multiband electronic system with local CDW fluctuations[15–17, 20] above T_{CDW}, such as 2H-Ta(Se,S)$_2$, the carrier scattering mechanism arises from collective excitations below the CDW and from local CDW fluctuations above the CDW.[19] Above T_{CDW} $\rho(T) \sim aT + b$, immediately below T_{CDW} $\rho(T) \sim dT^2$ and at temperatures below about 15–20 K $\rho(T) \sim cT^5$. The T^5 is due to normal electron–phonon scattering, whereas the T^2 arises due to scattering of electrons by collective excitations of CDW; the rapid drop just below CDW is due to CDW phase ordering. The linear terms a, b above T_{CDW} arise due to electron–phonon scattering and phase disorder impurity-like scattering due to local CDW fluctuations. The fits of resistivity for the entire single crystal alloy series of 2H-TaSe$_{2-x}$S$_x$ ($0 \leq x \leq 2$) are satisfactory (Fig. 4a–c, Table 2). In all samples resistivity is linear at high temperatures. Just above the superconducting T_c interband scattering is negligible and individual s-band and d-band normal electron–phonon scattering dominates.[19] The constant term b for such crystals is much smaller than for CDW samples, because disorder suppresses the CDW therefore increases the number of carriers and thus the conductivity.

We present the evolution of superconducting T_c in 2H-TaSe$_2$ with S substitution x (normalized to T_c value for $x = 0$) in Fig. 4d. The T_c shows 30-fold increase and anticorrelation with the evolution of the high-temperature local charge fluctuation parameter $b(x)$ (also normalized to b value for $x = 0$) (Fig. 4d). Note that weak decrease of T_c near $x = 1$ coincides with weak increase in normalized $b(x)$ near the same S content. It appears that the considerable increase and evolution of $T_c(x)$ is related to an increase in available carrier concentration or mobility. These changes are matched (Fig. 4d) with the nearly identical evolution
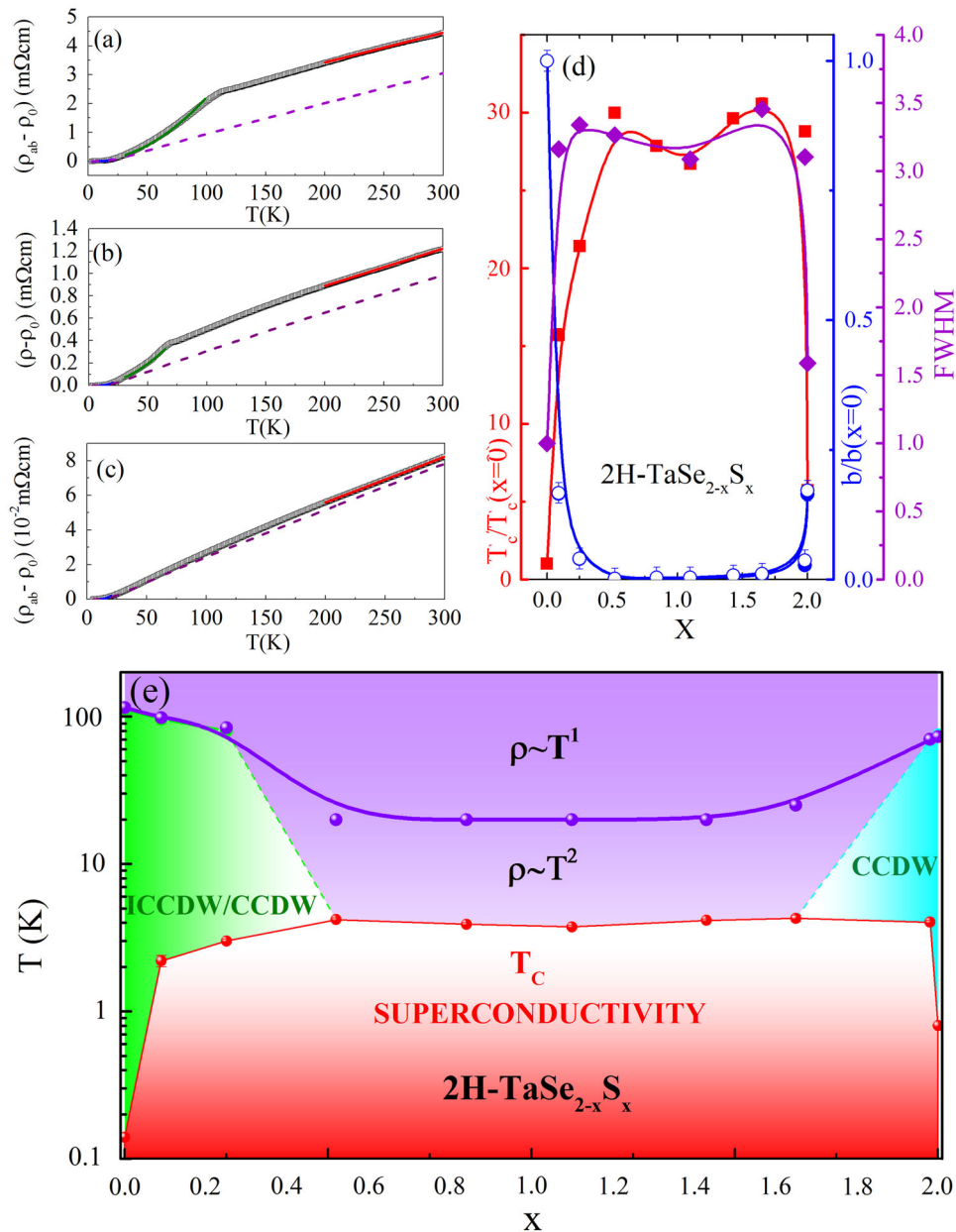
Fig. 4 Electronic phase diagram of 2H-TaSe$_{2-x}$S$_x$ ($0 \leq x \leq 2$) **a–c** Electronic scattering mechanism for **a** 2H-TaSe$_2$, **b** 2H-TaS$_2$, and **c** 2H-TaSe$_{0.9}$S$_{1.1}$. Low-temperature phonon scattering, scattering of collective excitations of CDW and high-temperature scattering of the local CDW fluctuations are shown by *blue*, *green*, and *red solid lines*, respectively. *Dashed violet line* shows the phonon resistivity approximated by the Bloch–Grüneisen formula (see text and Supplementary Information). **d** Note that the weak double dome evolution of superconducting $T_c(x)$ coincides with similar evolution of crystallographic disorder with sulfur content as revealed by FWHM of [006] Bragg peak in Fig. 1c. The intensity was normalized to 1 for each value of x. Moreover, $T_c(x)$ is in close correlation with disorder-induced changes in the high-temperature local charge fluctuations as seen by the changes in parameter b; all normalized to values of 2H-TaSe$_2$ ($x = 0$). The parameter b is shown from fits without (*open*) and with phonon subtraction from Bloch–Grüneisen formula (*full symbols*) (Supplementary Information). The error bars are about 0.01 for x, up to 0.04 for normalized T_c, and up to 0.01 for the normalized parameter b and FWHM (also see Table 1). **e** Phase diagram indicating the evolution of CDW (incommensurate ICCDW and commensurate CCDW) and superconductivity states with the change of x

of the crystallographic disorder as shown by the width of diffraction peaks taken on single crystals full width at half maximum (FWHM) normalized to width of $x = 0$ crystal. The linear resistivity $aT + b$ in the high-T_c crystals without CDW is rather close to the Bloch–Grüneisen phonon resistivity (Fig. 4c, Supplementary Information), suggesting that the strong suppression of parameter $b(x)$ in 2H-TaSe$_{2-x}$S$_x$ can be attributed to suppression of local CDW fluctuations for high-T_c crystals.

Figure 4e presents the electronic phase diagram. With the increase in x, the CDW transition of 2H-TaSe$_2$ is suppressed, whereas the superconducting transition temperature T_c increases up to 4.2 K for $x = 0.52$ where CDW disappears. Further sulfur increase shows weak but well resolved minimum in $T_c(x)$ for $x = 1.10$ up to the second maximal value of 4.28 K for $x = 1.65$ sulfur content in 2H-TaSe$_{1-x}$S$_x$. Signature of a CDW state, most probably CDW of the pure 2H-TaS$_2$, appears in $\rho(T)$ for higher S content up

Table 2. Superconducting T_c (defined as 90% of normal state resistivity; Fig. 2d), charge density wave T_{CDW} transition temperatures (defined as peak in resistivity; Fig. 2b, c), and fitting parameters of the CDW phase fluctuations scattering model for resistivity (see text)

x	T_c (K)	T_{CDW} (K)	c	c_{range} (K)	d	d_{range} (K)	a	b	L_{range} (K)	ρ_0
0	0.14	112(1)	2.12(7)	3–20	22.1(2)	30–100	102.8(1)	1.37(1)	200–300	3.4(5)
0.09(1)	2.2(1)	96(3)	0.52(2)	3–20	5.43(5)	34–86	22.4(3)	0.226(7)	200–300	1.1(2)
0.25(1)	3.0(5)	80(3)	0.27(2)	5–20	2.17(3)	34–65	8.08(1)	0.054(1)	200–300	0.9(1)
0.52(1)	4.2(1)	–	0.04(1)	5–20	–		1.6(1)	0.0004(1)	200–300	0.19(3)
0.84(1)	3.9(1)	–	0.10(1)	5–20	–		4.64(1)	0.0015(1)	200–300	0.8(1)
1.10(1)	3.7(2)	–	0.030(3)	5–20	–		2.64(1)	0.0031(1)	200–300	0.48(7)
1.43(1)	4.1(2)	–	0.20(1)	5–20	–		6.32(1)	0.0066(1)	200–300	1.1(1)
1.65(1)	4.3(1)	–	0.14(1)	5–20	–		6.82(1)	0.0099(3)	200–300	1.0(1)
1.98(1)	4.0 (1)	70(3)	0.20(1)	5–20	3.19(4)	30–60	16.8(1)	0.037(1)	200–300	0.36(5)
2.00(1)	0.8	75(1)	0.79(3)	3–20	7.78(3)	30–64	34.3(2)	0.225(1)	200–300	2.7(4)

Note: Considerable change in local CDW fluctuation scattering for crystals without CDW strives to increase conduction and is concomitant with the greatly enhanced superconducting T_c values. The units for c, d and a are in (10^{-8} mΩcm/K^5), (10^{-5} mΩcm/K^2), (10^{-4} mΩcm/K), respectively. The units for b and ρ_0 are in (mΩcm) and (10^{-1} mΩcm). For crystals near the middle of the alloy series where CDW cannot be detected in resistivity, the highest crystallographic disorder and consequently a substantial increase of ρ_0 (i.e., total $\rho(T)$ when $T\rightarrow 0$) are expected. However, the impurity-like scattering due to local CDW fluctuations (phase disorder scattering) term b becomes small for that range of x, making the overall resistivity ρ_0 smaller or similar to $x=0$ and $x=2$ crystals (Table 2, Columns b and ρ_0). L_{range} denotes the temperature range of linear $aT+b$ fit

to $x=2$. The two T_c maxima in the double-dome appear at the critical doping, where CDW orders vanish similar to 1T-Se$_2$ and 2H-NbSe$_2$.[25, 26]

DISCUSSION

It should be noted that electron-irradiated 2H-TaSe$_2$ shows enhancement of superconducting T_c up to about 2.5 K.[27] Irradiation introduces defects, i.e., changes in stoichiometry similar to chemical substitutions. Cu-intercalated 2H-TaS$_2$ shows enhancement of T_c up to 4.7 K.[28] Copper behaves as *n*-type dopant and therefore its intercalation brings both disorder and charge transfer.[29] Similar doping and disorder interplay is expected with Na intercalation in 2H-TaS$_2$, where T_c was raised up to 4.4 K.[30] In contrast, isoelectronic substitution in 2H-TaSe$_{2-x}$S$_x$ single crystal alloy series allows for clear separation of disorder from doping-induced changes. The basic electronic structure of 2H-TaSe$_2$, 2H-TaSeS, and 2H-TaS$_2$ is quite similar as shown in the Local Density Approximation (LDA) calculations (Supplementary Material), leaving disorder as the origin of the increase in T_c. The intense variation of physical properties at low energy is a prime example of emergent phenomena.

Below the CDW transition temperature, a gap opens in 2H-TaSe$_2$ on two distorted sublattices in contrast to undistorted sublattice.[15] This makes for a small density of states at the Fermi level and consequently low superconducting T_c.[10] Sulfur substitution could introduce different Ta–S and Ta–Se bond lengths, disorder and puckering of metal plane. This would suppress CDW and increase density of electronic states, electron–phonon coupling, and superconducting T_c.[31] The lattice defect disorder increases superconducting T_c in CDW superconductor ZrTe$_3$ by factor of only 2–3.[32] Furthermore, $T_c(x)$ (Fig. 4e) cannot be explained by the *f*-wave model of CDW that predicts linear $T_c(x)$ in 2H-TaSe$_{2-x}$S$_x$ ($0 \leq x \leq 2$), whereas increased conductivity in high-T_c crystals argues against the change of the amplitude of ionic vibrations as in disordered films or amorphous lattices.[33, 34]

The normal state properties of this material are not well understood theoretically. Our experimental results indicate that the low-temperature specific heat coefficient of the alloy is very close to that computed in LDA (please see Supplementary Material), suggesting that the correlations due to Coulomb interactions are weak, while the electron–phonon coupling couples strongly to a few states not too close to the Fermi surface, which is consistent with the results of ref. 35. Alternatively, strong correlations are invoked in the exciton liquid model of 2H-TaSe$_2$. This model of CDW in 2H-TaSe$_2$ provides an explanation of some anomalous normal state properties such as linear resistivity above CDW transition, pseudogap, optical conductivity $\sigma(\omega,T)$, and incoherent metal features.[20, 36] Within that model and in contrast to ZrTe$_3$,[32] emergence of CDW reduces incoherent scattering, i.e., CDW-related bump in $\rho(T)$ is a coherence restoring transition that enables higher conductivity below T_{CDW}. The reduction in interband mixing dispersion that mixes the small number of d_{z2} electrons and p_z holes should remove the CDW, maximizing strong scattering of preformed incoherent excitons and enabling linear resistivity to progress to lower temperatures.[20] The observation of wide temperature range of linear resistivity in high-T_c crystals (Fig. 2a) suggests the rapid reduction in conduction and valence band mixing within that model. This calls for photoemission studies of newly synthesized alloy to test these theoretical models and to clarify the measure of the correlation strength.

Pressure should bring phonon hardening following the contraction of lattice parameters from 2H-TaSe$_2$ to 2H-TaS$_2$ (Fig. 1).[23, 37, 38] Assuming similar bulk modulus to WSe$_2$ (72 GPa),[39] the estimated chemical pressure differences of 2H-TaSeS ($T_c = 3.7$ K) when compared with 2H-TaSe$_2$ ($T_c = 0.14$ K) and 2H-TaS$_2$ ($T_c = 0.8$ K) are 6 GPa (positive pressure/contraction) and 2.8 GPa (negative pressure/expansion). Positive pressure increases considerably superconducting T_c in both 2H-TaS$_2$ and 2H-TaS$_2$; 6 GPa brings T_c in 2H-TaSe$_2$ up to about 3 K.[40] CDW is robust, surviving up to 20 GPa (2H-TaSe$_2$) and up to 16 GPa (2H-TaS$_2$). Clearly, chemical pressure may influence the rise of superconducting T_c in S-doped 2H-TaSe$_2$, but it cannot explain the absence of CDW in high-T_c samples in the phase diagram (Fig. 4e), the increase of superconducting T_c with lattice expansion in 2H-TaS$_2$ or the $T_c(x)$ evolution in 2H-TaSe$_{2-x}$S$_x$ ($0 \leq x \leq 2$) (Fig. 4e). The reduction in conduction and valence band mixing within DMFT framework facilitates not only the reduction of incoherence and stabilization of pseudogap characterized by linear $\rho(T)$, but also an increase in density of states at the Fermi level, thus highlighting

the effect of disorder, incoherent states, and the importance of local dynamical correlations.[20]

In summary, we show that disorder-induced superconducting states arise by isoelectronic substitution in 2H-TaSe$_2$. In contrast to all known CDW superconductors that have hitherto featured only a single dome of T_c with variation of any external parameter, the electronic phase diagram we present features a weak double dome in $T_c(x)$. The increase in superconducting T_c and changes in $T_c(x)$ are directly correlated with crystallographic disorder and disorder-induced scattering of the local CDW fluctuations. Our experimental findings can be understood on more general grounds without relying on a specific microscopic theory. For a given band structure, weak disorder does not affect the superconductivity of an s-wave superconductor (Anderson's theorem, Supplementary Information),[1, 23] but it is detrimental to the competing CDW order. The combination of these effects results in an enhanced superconducting critical temperature and a reduction of the CDW.

METHODS

Single crystals of 2H-TaSe$_{2-x}$S$_x$ ($0 \leq x \leq 2$) were grown via iodine vapor transport method. The source and growth zone were set at 900 °C for 3 days and then kept at 900 and 800 °C, respectively, for 10 days. Black plate-like single crystals with a typical size of $3 \cdot 3 \cdot 0.2$ mm^3 were obtained. The element analysis was performed using an energy-dispersive X-ray spectroscopy in a JEOL LSM-6500 scanning electron microscope. Electrical resistivity, specific heat, and magnetization measurements were performed in a Quantum Design PPMS-9 and MPMS XL-5. XRD patterns on single crystals were taken using a Rigaku Miniflex. Room temperature powder XRD measurements were carried out at the X-ray powder diffraction (28-ID-C) beam line at National Synchrotron Light Source II. The raw room temperature powder X-ray 2D data were integrated and converted to intensity vs. scattering angle using the software Fit2D.[41] The average structure was assessed from raw diffraction data using the General Structure Analysis System operated under EXPGUI utilizing $P6_3/mmc$ model from the literature.[42–44]

AUTHOR CONTRIBUTIONS

C.P. designed research. L.L. and Y.L. made crystals and carried out transport, magnetization, and thermal measurements. L.L. and Y.S. contributed single crystal X-ray diffraction data. Y.L., Y.H., and J.W. performed SEM measurements. Z.W. and Y.Z. performed TEM measurements. M.A., E.D., A.T., E.S.B., and S.J.L.B. carried out and analyzed powder X-ray diffraction data. C.P. supervised the project, analyzed the transport data with Y.L. and single crystal data with L. L. and wrote the paper with L.L. and with contributions from G.K. and Y.S. X.D. performed the LDA calculations and contributed to the theoretical interpretation of results. The manuscript reflects contribution and ideas of all authors.

COMPETING INTERESTS

The authors declare no competing interest.

REFERENCES

1. Anderson, P. Absence of diffusion in certain random lattices. *Phys. Rev.* **109**, 1492–1505 (1958).
2. Belitz, D. & Kirkpatrick, T. R. The Anderson-Mott transition. *Rev. Mod. Phys.* **66**, 261–380 (1994).
3. Zeljkovic, I. *et al.* Imaging the impact of single oxygen atoms on superconducting Bi$_{2+y}$Sr$_{2-y}$CaCu$_2$O$_{8+x}$. *Science* **337**, 320–323 (2012).
4. Seo, S. *et al.* Disorder in quantum critical superconductors. *Nat. Phys.* **10**, 120–125 (2014).
5. Mizykami, Y. *et al.* Disorder-induced topological change of the superconducting gap structure in iron pnictides. *Nat. Commun.* **5**, 5657 (2014).
6. Alloul, H. *et al.* Defects in correlated metals and superconductors. *Rev. Mod. Phys.* **81**, 45–108 (2009).
7. Grüner, G. The dynamics of charge-density waves. *Rev. Mod. Phys.* **60**, 1129–1181 (1988).
8. Kiss, T. *et al.* Charge-order-maximized momentum dependent superconductivity. *Nat. Phys.* **3**, 720–725 (2007).
9. Borisenko, S. V. *et al.* Two energy gaps and Fermi-surface "arcs" in NbSe$_2$. *Phys. Rev. Lett.* **102**, 166402 (2009).
10. Harper, J. M., Geballe, T. E. & Disalvo, F. J. Thermal properties of layered transition-metal dichalcogenides at charge-density-wave transitions. *Phys. Rev. B* **15**, 2943–2951 (1977).
11. Moncton, D. E., Axe, J. D. & DiSalvo, F. J. Study of superlattice formation in 2H-NbSe$_2$, and 2H-TaSe$_2$ by neutron scattering. *Phys. Rev. Lett.* **34**, 734–737 (1975).
12. Nishihara, H., Scholz, G. A., Naito, M., Frindt, R. F. & Tanaka, S. NMR of ^{181}Ta in 2H-TaS$_2$ and 2H-TaSe$_2$, observation of locally commensurate CDW. *J. Magn. Magn. Mater.* **31**, 717–718 (1983).
13. Laverock, J. *et al.* k-resolved susceptibility function of 2H-TaSe$_2$ from angle-resolved photoemission. *Phys. Rev. B* **88**, 035108 (2013).
14. Van Wezel, J. Polar charge and orbital order in 2H-TaS$_2$. *Phys. Rev. B* **85**, 035131 (2012).
15. Barnett, R. L., Polkovnikov, A., Demler, E., Yin, Wei-Guo & Ku, Wei Coexistence of gapless excitations and commensurate charge-density wave in the 2H transition metal dichalcogenides. *Phys. Rev. Lett.* **96**, 026406 (2006).
16. Vescoli, V., Degiorgi, L., Berger, H. & Forró, L. Dynamics of correlated two-dimensional materials: the 2H-TaSe$_2$ case. *Phys. Rev. Lett.* **81**, 453–456 (1998).
17. Ruzicka, B., Degiorgi, L., Berger, H., Gaál, R. & Forró, L. Charge dynamics of 2H-TaSe$_2$ along the less conducting c-axis. *Phys. Rev. Lett.* **86**, 4136–4139 (2001).
18. Yokota, K. I., Kurata, G., Matsui, T. & Fukuyama, H. Superconductivity in the quasi-two-dimensional conductor 2H-TaSe$_2$. *Phys. B* **284-288**, 551–552 (2000).
19. Naito, M. & Tanaka, S. Electrical transport properties in 2H-NbS$_2$, -NbSe$_2$, -TaS$_2$ and -TaSe$_2$. *J. Phys. Soc. Jpn.* **51**, 219–227 (1982).
20. Tarapder, A., Koley, S., Vidhyadhiraja, N. S. & Laad, M. S. Preformed excitonic liquid route to a charge density wave in 2H-TaSe$_2$. *Phys. Rev. Lett.* **106**, 236405 (2011).
21. Xu, W., Haule, K. & Kotliar, G. Hidden Fermi liquid, scattering rate saturation and Nernst effect: a dynamical mean field theory perspective. *Phys. Rev. Lett.* **111**, 036401 (2013).
22. Deng, X., Mravlje, J., Zitko, R., Ferrero, M., Kotliar, G. & Georges, A. How bad metals turn good: spectroscopic signatures of resilient quasiparticles. *Phys. Rev. Lett.* **110**, 086401 (2013).
23. Anderson, P. W. Theory of dirty superconductors. *J. Phys. Chem. Solids* **11**, 26–30 (1959).
24. McMillan, W. L. Transition temperature of strong-coupled superconductors. *Phys. Rev.* **167**, 331–344 (1968).
25. Kusmartseva, A. F., Sipos, B., Berger, H., Forró, L. & Tutiš, E. Pressure induced superconductivity in pristine 1T-TiSe$_2$. *Phys. Rev. Lett.* **103**, 236401 (2009).
26. Feng, Y. *et al.* Order parameter fluctuations at a buried quantum critical point. *Proc. Natl. Acad. Sci.* **109**, 7224–7229 (2012).
27. Mutka, H. Superconductivity in irradiated charge-density-wave compounds 2H-NbSe$_2$, 2H-TaS$_2$, and 2H-TaSe$_2$. *Phys. Rev. B* **28**, 2855–2858 (1983).
28. Wagner, K. E. *et al.* Tuning the charge density wave and superconductivity in Cu$_x$TaS$_2$. *Phys. Rev. B* **78**, 104520 (2008).
29. Zhao, J. F. *et al.* Evolution of the electronic structure of 1T-Cu$_x$TiSe$_2$. *Phys. Rev. B* **99**, 146401 (2007).
30. Fang, L. *et al.* Fabrication and superconductivity of Na$_x$TaS$_2$ crystals. *Phys. Rev. B* **72**, 014534 (2005).
31. Liu, Y. *et al.* Nature of charge-density-wave and superconductivity in 1T-TaSe$_{2-x}$Te$_x$. *Phys. Rev. B* **94**, 041531 (2016).
32. Zhu, X. *et al.* Disorder-induced bulk superconductivity in ZrTe$_3$ single crystals via growth control. *Phys. Rev. B* **87**, 024508 (2013).
33. Castro Neto, A. H. Charge density wave, superconductivity, and anomalous metallic behavior in 2D transition metal dichalcogenides. *Phys. Rev. Lett.* **86**, 4382–4385 (2001).
34. Garland, J. W., Bennemann, K. H. & Mueller, F. M. Effect of lattice disorder on the superconducting transition temperature. *Phys. Rev. Lett.* **21**, 1315–1319 (1968).
35. Varma, C. M. & Simons, A. L. Strong coupling theory of charge-density-wave transitions. *Phys. Rev. Lett.* **51**, 138–141 (1983).
36. Borisenko, S. V. *et al.* Pseudogap and charge density waves in two dimensions. *Phys. Rev. B* **100**, 196402 (2008).
37. Loa, I. & Syassen, K. Calculated elastic and electronic properties of MgB$_2$ at high pressures. *Solid State Comm.* **118**, 279–282 (2001).

38. Smith, T. F., Shelton, R. N. & Schwall, R. E. Superconductivity of TaSe$_{2-x}$Se$_x$ layer compounds at high pressure. *J. Phys. F: Metal. Phys.* **5**, 1713–1725 (1975).

39. Selvi, E., Aksoy, R., Knudson, R. & Ma, Y. High-pressure X-ray diffraction study of tungsten diselenide. *J. Phys. Chem. Solids* **69**, 2311–2314 (2008).

40. Freitas, D. C. et al. Strong enhancement of superconductivity at high pressures within the charge-density-wave states of 2H-TaS$_2$ and 2H-TaSe$_2$. *Phys. Rev. B* **93**, 184512 (2016).

41. Hammersley, A. P., Svensson, S. O., Hanfland, M., Fitch, A. N. & Hausermann, A. Two-dimensional detector software: from real detector to idealised image or two-theta scan. *High Pressure Res.* **14**, 235–248 (1996).

42. Larson, A.,C. and Von Dreele, R.,B. Report No. LAUR-86-748, Los Alamos National Laboratory, Los Alamos, NM 87545 (2004).

43. Toby, B. H. EXPGUI, a graphical user interface for GSAS. *J. Appl. Crystallogr.* **34**, 210–213 (2001).

44. Brixner, L. H. Preparation and properties of the single crystalline AB$_2$-type selenides and tellurides of niobium, tantalum, molybdenum and tungsten. *J. Inorg. Nucl. Chem.* **24**, 257–263 (1962).

Supplementary Information accompanies the paper on the *npj Quantum Materials* website (doi:10.1038/s41535-017-0016-9).